Article ID：1007−7294(2025)06−0849−14

Fixed-time Target-guided Coordinate Control of Unmanned Surface Vehicles Based on Dynamic Surface Control

LI Chao−yi[2], *XU Hai−xiang*[1,2,3], *YU Wen−zhao*[1,2,3], *DU Zhe*[1,2], *DING Ya−nan*[2]

(1. Key Laboratory of High Performance Ship Technology (Wuhan University of Technology), Ministry of Education, Wuhan 430062, China; 2. School of Naval Architecture, Ocean and Energy Power Engineering, Wuhan University of Technology, Wuhan 430062, China; 3. Sanya Science and Education Innovation Park of Wuhan University of Technology, Sanya 572024, China)

Abstract: This paper presents an investigation on the target-guided coordinated control (TACC) of unmanned surface vehicles (USVs). In the scenario of tracking non-cooperative targets, the status information of the target can only be obtained by some USVs. In order to achieve semi-encirclement tracking of non-cooperative targets under maritime security conditions, a fixed-time tracking control method based on dynamic surface control (DSC) is proposed in this paper. Firstly, a novel TACC architecture with decoupled kinematic control law and decoupled kinetic control law was designed to reduce the complexity of control system design. Secondly, the proposed DSC-based target-guided kinematic control law including tracking points pre-allocation strategy and sigmoid artificial potential functions (SigAPFs) can avoid collisions during tracking process and optimize kinematic control output. Finally, a fixed-time TACC system was proposed to achieve fast convergence of kinematic and kinetics errors. The effectiveness of the proposed TACC approach in improving target tracking safety and reducing control output chattering was verified by simulation comparison results.

Key words: unmanned surface vehicle; distributed control; target-guided coordinate control; fixed-time convergence; dynamic surface control

CLC number： TP273 U664.82 **Document code：** A **doi:** 10.3969/j.issn.1007−7294.2025.06.001

0 Introduction

The utilization and exploration of ocean resources and the escort of important shipping lanes have attracted full attention around the world[1]. In order to effectively protect maritime territory and cooperative targets from infringement, path-guided coordinate control[2−3], trajectory-guided coordinate control[4−5], target-guided coordinate control[6] and collaborative target surrounding[7−8] have become important working modes for multiple USVs. In particular, collaborative target tracking control technology of USVs has gained broad applications in formation escort, maritime patrol and intrusion target expulsion.

Received date：2024−12−21

Foundation item：Supported by the National Natural Science Foundation of China (52201373) and the Hainan Provincial Joint Project of Sanya Yazhou Bay Science and Technology City (2021CXLH0016)

Biography：LI Chao-yi(1996–), male, Ph.D candidate; XU Hai-xiang(1975–), male, Ph.D., professor; YU Wen-zhao(1989–), male, Ph.D., associate research fellow, corresponding author, E-mail: wzyu@whut.edu.cn; DU Zhe(1993–), male, Ph.D., lecturer; DING Ya-nan(1998–), female, master student.

During the past few years, research on USVs TACC has made great progress. Fahimi[9] transformed the formation tracking problem into the virtual target tracking problem. By designing a sliding mode controller to track the position and heading of a virtual target, formation maintenance was achieved during the movement of USVs. Works on decentralized control for tracking a cooperative target was discussed in Refs. [10−13]. In Ref. [10], NN was developed to estimate model uncertainties and external environmental disturbance. Meanwhile, dynamic surface control technology was utilized in the kinematic control layer to smooth the kinetic control output chattering. To avoid actuator saturation, Khoshnam[11] introduced a generalized saturation function into the kinetic error and further used RBFNN based on Ref. [10] to accurately estimate internal and external disturbances. To address the problems of angle constraints and actuator faults, barrier Lyapunov functions (BLFs) were designed in Ref. [12], and the finite time convergence of the control system was achieved. Sun et al[13] developed a continuous function to replace the signum function in the sliding mode control method, which effectively reduced the chattering based on Ref. [9]. Different from those in Refs. [10−13], Liu et al[14] studied the problem of unavailable non-cooperative target velocity. An extended state observer (ESO) was designed in the kinematic control law to estimate the uncertain target dynamics due to the unavailable velocity.

However, the above studies are all based on decentralized control structures. Since there is no information exchange between USVs, the tracking synchronization is not optimal. Based on the above issues, the control structure of USVs TACC gradually transitions from decentralized to distributed[15−20]. On the basis of Ref. [14], Gao et al[15] introduced an event triggering mechanism in the distributed ESO (DESO) to simultaneously deal with the problem of target state unavailable and communication delay. Considering the unknown obstacles during target tracking, Gao et al[16] added a control barrier function (CBF) as a solution into the kinematic control law in Ref. [15]. In Ref. [17], a potential function was designed to avoid collisions between USVs and targets. Meanwhile, the event-trigger scheme was introduced into the kinematic layer, which could reduce the actuator activity. Considering that only some USVs could obtain position information of the target under different scenarios, Ma et al[18] further proposed a switched topology DESO based on the works in Ref. [14] and Ref. [15]. Different from Ref. [18], Zhu et al[19] proposed three substitution strategies for the substitution problem of damaged USV individuals to ensure the continuation of the tracking task. Considering the convergence speed of the tracking system, Zhu et al[20] designed three new initial USVs selection strategies to achieve fast implementation of tracking tasks in the case of USVs redundancy. On the other hand, finite-time convergence was also achieved in the proposed control system.

Motivated by the mentioned works, this paper is aimed to propose a novel TACC method for USVs. The highlights of the study cover: (i) division of the TACC architecture into two parts, including decoupled kinematic control layer and kinetic control layer, designed to reduce the complexity of control system design, (ii) proposal of a DSC-based target-guided kinematic control law including tracking points pre-allocation strategy and sigmoid-APFs to avoid collisions during tracking process and optimize kinematic control output chattering, (iii) proposal of a fixed-time TACC system to make errors converge fast, and estimation of time-varying unknown sideslip angle and external environmental disturbance by utilizing fixed-time ESO and Chebyshev orthogonal neural network (CONN) estimator, respectively.

Compared with the existing research, the salient features of the proposed method are as follows: (i) different from Refs. [15–20], not only the kinematic control layer is decoupled from the kinetic control layer, but also the velocity synchronization control objective is considered, which reduces the complexity of the system design and makes it more suitable for engineering practice, (ii) different from the one-line formation in Refs. [14, 18] and the triangle formation in Refs. [9–11, 13, 17] and the quadrangle formation in

Refs. [15, 16], a semi-encirclement tracking formation for the patrol and eviction conditions of suspicious targets at sea is proposed; different from Refs. [16] and [17], the collision avoidance constraints and connectivity maintenance constraints between individuals are considered, and a monotonic and bounded APFs is utilized based on sigmoid function, which effectively ensures the safety of the whole tracking process, (iii) based on the finite-time form in Refs. [12] and [20], the fixed-time TACC system is further designed and the stability is analyzed through the Lyapunov theory.

1 Preliminaries and problem formulation

In this paper, the following notations are used. Given any $\varpi > 0$, it follows that $\mathrm{sig}(\cdot) = |\cdot|^{\varpi}\mathrm{sgn}(\cdot)$. $\max\{\cdot\}$ denotes the maximum value in the array.

1.1 Graph theory

The communication topology is described by a graph $\boldsymbol{G} = \{\boldsymbol{V}, \boldsymbol{\xi}\}$, where $\boldsymbol{V} = \{n_0, \cdots, n_N\}$ is a node set and $\boldsymbol{\xi} = \{(n_i, n_j) \in \{n_1, ..., n_N\} \times \boldsymbol{V}\}$ is an edge set. The links among N USVs is defined as $\boldsymbol{A} = [a_{ij}] \in \Re^{N\times N}(j > 0)$. If $(n_i, n_j) \in \boldsymbol{\xi}$, $a_{ij} = 1$, otherwise, $a_{ij} = 0$. The virtual links between USVs and the non-cooperative target is defined as $\boldsymbol{B} = [a_{i0}] \in \Re^{N\times 1}$. If the ith USV can obtain the status information of the non-cooperative target, $a_{i0} = 1$, otherwise, $a_{i0} = 0$.

1.2 Kinematic and kinetic models for USVs

The kinematic mathematical model of the ith USV is described as:

$$\begin{cases} \dot{x}_i = u_i\cos(\psi_{bi}) - v_i\sin(\psi_{bi}) \\ \dot{y}_i = u_i\sin(\psi_{bi}) + v_i\cos(\psi_{bi}) \\ \dot{\psi}_{bi} = r_i \end{cases}, i = 1, 2, ..., N \tag{1}$$

where x_i, y_i, ψ_{bi} denote the position in surge, sway and yaw, respectively. u_i, v_i, r_i denote the velocity in surge, sway and yaw, respectively.

Introducing the sideslip angle in Eq. (1), it follows that:

$$\begin{cases} \dot{x}_i = U_i\cos(\psi_i) \\ \dot{y}_i = U_i\sin(\psi_i) \\ \dot{\psi}_i = r_i + \dot{\beta}_i \end{cases} \tag{2}$$

where $\beta_i = \arctan(v_i/u_i)$ is the sideslip angle.

The kinetic mathematical model of the ith USV is described as:

$$\begin{cases} \dot{u}_i = \dfrac{m_{22,i}}{m_{11,i}}v_i r_i - \dfrac{d_{11,i}}{m_{11,i}}u_i + \dfrac{\tau_{ui}}{m_{11,i}} + \dfrac{d_{wui}}{m_{11,i}} \\ \dot{v}_i = -\dfrac{m_{11,i}}{m_{22,i}}u_i r_i - \dfrac{d_{22}}{m_{33}}v_i + \dfrac{d_{wvi}}{m_{22,i}} \\ \dot{r}_i = \dfrac{m_{11} - m_{22}}{m_{33,i}}u_i v_i - \dfrac{d_{33,i}}{m_{33,i}}r_i + \dfrac{\tau_{ri}}{m_{33,i}} + \dfrac{d_{wri}}{m_{33,i}} \end{cases} \tag{3}$$

where $m_{11,i}$, $m_{22,i}$, $m_{33,i}$ are masses and $d_{11,i}$, $d_{22,i}$, $d_{33,i}$ are hydrodynamic damping coefficients for the corresponding freedom respectively. $\boldsymbol{\tau}_i^* = [\tau_{ui}, 0, \tau_{ri}]^{\mathrm{T}}$ denotes the control force and $\boldsymbol{d}_{wi} = [d_{wui}, d_{wvi}, d_{wri}]^{\mathrm{T}}$ is the time-varying disturbance.

1.3 Problem formulation

The semi-encirclement target tracking scene is shown in Fig. 1. OXY is the body-fixed coordinate and $O_{\mathrm{E}}X_{\mathrm{E}}Y_{\mathrm{E}}$ is the north-east-down coordinate. The ith USV position is defined as $\boldsymbol{p}_i = [x_i, y_i]^{\mathrm{T}} \in \Re^{2\times 1}$. The black circle outside the target indicates the desired tracking circle, and R_t indicates the tracking radius. The target initial heading is defined as ψ_t and position as $\boldsymbol{p}_t = [x_t, y_t]^{\mathrm{T}} \in \Re^2$. Four control objectives need to be met.

(1) Make sure the ith USV follows the target and stays at the tracking point.

$$\lim_{t\to\infty}\left\|\boldsymbol{p}_i-\boldsymbol{p}_t-\boldsymbol{p}_{it,d}\right\|\to 0 \tag{4}$$

where $\boldsymbol{p}_{it,d}$ is the desired distance between the ith USV and the tracking point.

(2) Make sure the ith USV follows the target velocity $\boldsymbol{v}_t=[u_t,v_t,r_t]^{\mathrm{T}}$.

$$\lim_{t\to\infty}\|\boldsymbol{v}_i-\boldsymbol{v}_t\|\to 0 \tag{5}$$

where u_t , v_t and r_t are the surge velocity, sway velocity and yaw velocity, respectively. $\boldsymbol{v}_i=[u_i,v_i,r_i]^{\mathrm{T}}$.

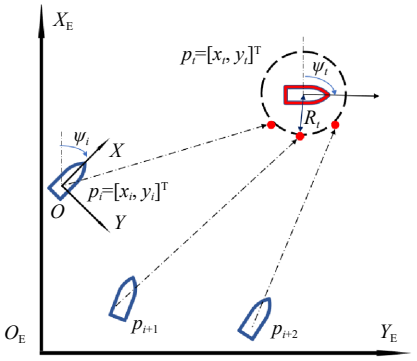

Fig.1 TACC system for USVs

(3) Make sure USVs do not collide with each other.

$$\left\|\boldsymbol{p}_i-\boldsymbol{p}_j\right\|\geqslant R_{a1},\ j=1,2,...,N+1,\ j\neq i \tag{6}$$

(4) Make sure each USV is within the effective communication distance.

$$\left\|\boldsymbol{p}_i-\boldsymbol{p}_j\right\|\leqslant R_{c2},\ j=1,2,...,N,\ j\neq i \tag{7}$$

where R_{c2} is the maximum connective distance.

1.4 Lemmas and assumptions

Lemma 1[21]: Consider the nonlinear function $\dot{x}=f(t,x)$. If there exists a continuous radially unbounded function $\boldsymbol{V}(x)$ such that $\boldsymbol{V}(x)=0\Leftrightarrow x=0$ and satisfies $\dot{\boldsymbol{V}}(x)\leqslant-\kappa_1\boldsymbol{V}^{\varepsilon_1}(x)-\kappa_2\boldsymbol{V}^{\varepsilon_2}(x)+\zeta$ for some $\kappa_1,\kappa_2,\zeta>0$, $\varepsilon_1\in(0,1)$ and $\varepsilon_2\in(1,\infty)$, then the origin of the system is globally actual fixed-time stable. Furthermore, given a scalar quantity $\varepsilon_3\in(0,1)$, the convergence time T satisfies $T\leqslant 1/(\kappa_1\varepsilon_3(1-\varepsilon_1))+1/(\kappa_2\varepsilon_3(\varepsilon_2-1))$.

Assumption 1: The target velocity is lower than USVs. The target initial heading can be obtained.

Assumption 2: The sideslip angle β_i satisfies $|\beta_i|\leqslant\beta^*$ with $\beta^*>0$.

2 Target tracking points pre-allocation

To avoid conflicts, tracking points need to be evenly distributed over the semi-encirclement. The specific scenario is shown in Fig. 2. The position of the tracking points is determined by the target's initial heading $\psi_t(0)$, the target's initial position $\boldsymbol{p}_t(0)=[x_t(0),y_t(0)]^{\mathrm{T}}$ and the radius of the semi-encirclement circle R_t. The tracking points are defined as $\boldsymbol{p}_{tk}=[x_{tk},y_{tk}]^{\mathrm{T}},k=1,2,...,N$, the calculation method is as follows:

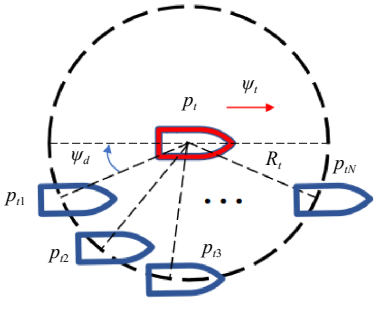

Fig.2 Tracking points allocation strategy

$$\begin{cases}x_{tk}=x_t(0)+R_t\times\cos(\psi_t(0)+\pi+\psi_d)\\ y_{tk}=y_t(0)+R_t\times\sin(\psi_t(0)+\pi+\psi_d)\end{cases},k=1,2,\ldots,N \tag{8}$$

where $\psi_d=\pi/(N+1)$.

After the tracking points are determined, the negotiation method is needed to assign the tracking points to USVs. The distance is defined between the ith USV and the kth tracking point as d_{ik}, which can be further expressed as:

$$d_{ik}=\sqrt{(x_i-x_{tk})^2+(y_i-y_{tk})^2},\ \ i,k=1,2,\ldots,N \tag{9}$$

By determining $\min\{d_{ik}\}$, the kth tracking point is allocated to the ith USV, and the allocation process is

repeated for the remaining tracking points and USVs until all allocations are completed. It is worth noting that when a tracking point is allocated to multiple USVs at the same time, it should be allocated to the farthest USV before continuing with subsequent allocation tasks.

Based on the above strategy, the matching matrix between USV individuals and tracking points can be defined as $\boldsymbol{D}^* \in \Re^{N\times 2}$, which is further used in the design of the kinematic control law.

3 Distributed fixed-time collaborative controller design

3.1 Fixed-time kinematic control law design

Combining the graph theory, the kinematic control error is given as follows:

$$\begin{cases} \boldsymbol{e}_{ti} = \boldsymbol{e}_{pi} + \boldsymbol{e}_{vi} \\ \boldsymbol{e}_{pi} = \boldsymbol{R}_i^{\mathrm{T}}(\psi_i)\left[\sum\limits_{j=1}^{N} a_{ij}(\boldsymbol{p}_i - \boldsymbol{p}_j - \boldsymbol{p}_{ij,d}) + a_{i0}(\boldsymbol{p}_i - \boldsymbol{p}_t - \boldsymbol{p}_{it,d})\right] \\ \boldsymbol{e}_{vi} = \boldsymbol{R}_i^{\mathrm{T}}(\psi_i)\left[\sum\limits_{j=1}^{N} a_{ij}(\dot{\boldsymbol{p}}_i - \dot{\boldsymbol{p}}_j) + a_{i0}(\dot{\boldsymbol{p}}_i - \dot{\boldsymbol{p}}_t)\right] \\ \boldsymbol{R}_i(\psi_i) = \begin{bmatrix} \cos(\psi_i) & -\sin(\psi_i) \\ \sin(\psi_i) & \cos(\psi_i) \end{bmatrix} \end{cases} \tag{10}$$

where $\boldsymbol{e}_{pi}$ is the position tracking error, $\boldsymbol{e}_{vi}$ is the velocity tracking error, $\boldsymbol{p}_{ij,d}$ is the desired distance between USVs, $\boldsymbol{p}_{it,d} = \boldsymbol{p}_{t\boldsymbol{D}_{ik}^*} - \boldsymbol{p}_t$ is the desired distance among USVs and target, $\boldsymbol{p}_{t\boldsymbol{D}_{ik}^*}$ is the kth tracking point position corresponding to the ith USV, and $\boldsymbol{R}_i$ is the coordinate rotation matrix.

Remark 1: Considering that the velocity of the non-cooperative target is unavailable, the velocity synchronization error is calculated by using the change rate of the target position in the north-east-down coordinate, and then converted to the body-fixed coordinate for kinematic control error calculation.

The time derivative of Eq. (10) is given as follows:

$$\begin{cases} \dot{\boldsymbol{e}}_{ti} = -\dot{\psi}_i \boldsymbol{S}\boldsymbol{e}_{ti} + \sum\limits_{j=0}^{N} a_{ij}\begin{bmatrix} u_i \\ v_i \end{bmatrix} + \sum\limits_{j=0}^{N} a_{ij}\dot{\psi}_i \boldsymbol{S}\begin{bmatrix} u_i \\ v_i \end{bmatrix} - \left(\sum\limits_{j=1}^{N} a_{ij}\boldsymbol{R}_i^{\mathrm{T}}\boldsymbol{R}_j + \sum\limits_{j=1}^{N} a_{ij}\dot{\psi}_i \boldsymbol{S}\boldsymbol{R}_i^{\mathrm{T}}\boldsymbol{R}_j\right)\begin{bmatrix} u_j \\ v_j \end{bmatrix} - \\ \qquad a_{i0}\boldsymbol{R}_i^{\mathrm{T}}\dot{\boldsymbol{p}}_t - \sum\limits_{j=0}^{N} a_{ij}\dot{\boldsymbol{v}}_i + \sum\limits_{j=1}^{N} a_{ij}\boldsymbol{R}_i^{\mathrm{T}}\boldsymbol{R}_j\dot{\boldsymbol{v}}_j - a_{i0}\boldsymbol{R}_i^{\mathrm{T}}\ddot{\boldsymbol{p}}_t \\ \boldsymbol{S} = \begin{bmatrix} 0 & -1 \\ 1 & 0 \end{bmatrix} \end{cases} \tag{11}$$

An auxiliary variable $\bar{\boldsymbol{\delta}}_0 = [-\delta_0, 0]^{\mathrm{T}} \in \Re^2$ is introduced into Eq. (11) to solve the underactuated problem of USVs:

$$\bar{\boldsymbol{e}}_{ti} = \boldsymbol{e}_{ti} - \bar{\boldsymbol{\delta}}_0 \tag{12}$$

By defining $\boldsymbol{\sigma}_i = [u_i, r_i]^{\mathrm{T}}$ and $\boldsymbol{B}_i = \mathrm{diag}\{d_i, \delta_0\}$, substituting the differentiation of Eq. (12) into Eq. (11), it follows that:

$$\begin{aligned} \dot{\bar{\boldsymbol{e}}}_{ti} = & -\dot{\psi}_i \boldsymbol{S}\bar{\boldsymbol{e}}_{ti} + \begin{bmatrix} 0 \\ \sum\limits_{j=0}^{N} a_{ij}v_i + \delta_0\dot{\beta}_i \end{bmatrix} + \sum_{j=0}^{N} a_{ij}\dot{\psi}_i \boldsymbol{S}\begin{bmatrix} u_i \\ v_i \end{bmatrix} + \boldsymbol{B}_i\boldsymbol{\sigma}_i - (\dot{\psi}_i\boldsymbol{S} + \boldsymbol{I})\sum_{j=1}^{N} a_{ij}\boldsymbol{R}_i^{\mathrm{T}}\boldsymbol{R}_j\begin{bmatrix} u_j \\ v_j \end{bmatrix} - \\ & a_{i0}\boldsymbol{R}_i^{\mathrm{T}}\dot{\boldsymbol{p}}_t - \sum_{j=0}^{N} a_{ij}\dot{\boldsymbol{v}}_i + \sum_{j=1}^{N} a_{ij}\boldsymbol{R}_i^{\mathrm{T}}\boldsymbol{R}_j\dot{\boldsymbol{v}}_j - a_{i0}\boldsymbol{R}_i^{\mathrm{T}}\ddot{\boldsymbol{p}}_t \end{aligned} \tag{13}$$

where $\boldsymbol{I} \in \Re^{2\times 2}$ is identity matrix.

The potential function is further introduced in $\bar{\boldsymbol{e}}_{ti}$, the total error $\boldsymbol{q}_{ti}$ is defined as follows:

$$\begin{cases} \boldsymbol{q}_{ti} = \bar{\boldsymbol{e}}_{ti} - \boldsymbol{e}_{fi} \\ \boldsymbol{e}_{fi} = \boldsymbol{R}_i^{\mathrm{T}} \left(\sum\limits_{j=1}^{M} \dfrac{\partial V_{ij}^{\mathrm{a}}}{\partial \boldsymbol{p}_i} + \sum\limits_{k=1}^{M} \dfrac{\partial V_{ij}^{\mathrm{c}}}{\partial \boldsymbol{p}_i} \right) \end{cases} \tag{14}$$

where $\boldsymbol{e}_{fi}$ is the sum of the potential function gradients, V_{ij}^{a} is the inter-USVs collision avoidance potential function, V_{ij}^{c} is the connectivity constraint potential function. The latter two can be further described as

$$\begin{cases} \dfrac{\partial V_{ij}^{\mathrm{a}}}{\partial \boldsymbol{p}_i} = \begin{cases} \varepsilon_{ia} \times (R_{a2} - R_{a1}) \times \dfrac{e^{c_{ia} \times p_{ij}^2}}{(1 + \mathrm{e}^{c_{ia} \times p_{ij}^2})^2} \times (\boldsymbol{p}_i - \boldsymbol{p}_j), R_{a1} \leqslant p_{ij} \leqslant R_{a2} \\ \boldsymbol{0}_2, p_{ij} < R_{a1} \& p_{ij} > R_{a2} \end{cases} \\ \dfrac{\partial V_{ij}^{\mathrm{c}}}{\partial \boldsymbol{p}_i} = \begin{cases} \varepsilon_{ic} \times (R_{c2} - R_{c1}) \times \dfrac{e^{c_{ic} \times (R_{c2}^2 - p_{ij}^2)}}{(1 + \mathrm{e}^{c_{ic} \times (R_{c2}^2 - p_{ij}^2)})^2} \times (\boldsymbol{p}_i - \boldsymbol{p}_j), R_{c1} \leqslant p_{ij} \leqslant R_{c2} \\ \boldsymbol{0}_2, p_{ij} < R_{c1} \& p_{ij} > R_{c2} \end{cases} \end{cases} \tag{15}$$

where $p_{ij} = \left\| \boldsymbol{p}_i - \boldsymbol{p}_j \right\|$ denotes the distance between the ith and the jth USV, ε_{ia}, ε_{ic}, c_{ia}, c_{ic} are positive constants, R_{a2} is the maximum detection region, R_{a1} is the minimum detection region, and R_{c1} is the minimum connective distance. The details can be seen in Ref. [22].

The estimation errors of $z_{1i} = \hat{\psi}_i - \psi_i$ and $z_{2i} = \hat{\beta}_i - \beta_i$ are defined. To estimate β_i, a fixed-time ESO is developed as

$$\begin{cases} \dot{\hat{\psi}}_i = -k_\psi (\mathrm{sig}^{\alpha_\psi}(z_{1i}) + \mathrm{sig}^{\beta_\psi}(z_{1i})) + \hat{\beta}_i + r_i \\ \dot{\hat{\beta}}_i = -k_\beta (\mathrm{sig}^{\alpha_\psi}(z_{1i}) + \mathrm{sig}^{\beta_\psi}(z_{1i})) + \dot{\beta}_i \end{cases} \tag{16}$$

where k_ψ and k_β are positive parameters.

Combining Eqs. (13), (14) and (16), the fixed-time kinematic controller is designed as

$$\begin{aligned} \begin{bmatrix} u_{di} \\ r_{di} \end{bmatrix} = \boldsymbol{B}_i^{-1} \Bigg[& -\boldsymbol{k}_{t1} \mathrm{sig}^{\alpha_t}(\boldsymbol{q}_{ti}) - \boldsymbol{k}_{t2} \mathrm{sig}^{\beta_t}(\boldsymbol{q}_{ti}) + \sum_{j=0}^{N} a_{ij} \dot{\boldsymbol{v}}_i + a_{i0} \boldsymbol{R}_i^{\mathrm{T}} \dot{\boldsymbol{p}}_t - \sum_{j=1}^{N} a_{ij} \boldsymbol{R}_i^{\mathrm{T}} \boldsymbol{R}_j \dot{\boldsymbol{v}}_j + a_{i0} \boldsymbol{R}_i^{\mathrm{T}} \ddot{\boldsymbol{p}}_t + \\ & (\dot{\psi}_i \boldsymbol{S} + \boldsymbol{I}) \sum_{j=1}^{N} a_{ij} \boldsymbol{R}_i^{\mathrm{T}} \boldsymbol{R}_j \begin{bmatrix} u_j \\ v_j \end{bmatrix} - \sum_{j=0}^{N} a_{ij} \dot{\psi}_i \boldsymbol{S} \begin{bmatrix} u_i \\ v_i \end{bmatrix} - \begin{bmatrix} 0 \\ \sum\limits_{j=0}^{N} a_{ij} v_i + \delta_0 \dot{\beta}_i \end{bmatrix} \Bigg] \end{aligned} \tag{17}$$

where u_{di} is the desired surge velocity output and r_{di} is the desired angular velocity output; $\boldsymbol{k}_{t1}$ and $\boldsymbol{k}_{t2}$ are positive gains; $0 < \alpha_t < 1$, $\beta_t > 1$.

In order to smooth the kinematic output chattering caused by the acceleration signals of $\dot{\boldsymbol{v}}_i$, $\dot{\boldsymbol{v}}_j$ and $\ddot{\boldsymbol{p}}_t$, dynamic surface control technology is introduced in Eq. (17). The first-order low-pass filter is introduced.

$$T_d \dot{\tilde{\boldsymbol{v}}}_z + \tilde{\boldsymbol{v}}_z = \boldsymbol{v}_z, \quad \tilde{\boldsymbol{v}}_z(0) = \boldsymbol{v}_z(0), \quad z = 1, \ldots i, j, \ldots, N+1 \tag{18}$$

where T_d is the time constant, $\tilde{\boldsymbol{v}}_z$ is the filtered speed value of USVs and the target.

Substituting the differentiation of Eq. (18) into Eq. (17), it follows that:

$$\begin{aligned} \begin{bmatrix} u_{di} \\ r_{di} \end{bmatrix} = \boldsymbol{B}_i^{-1} [& -\boldsymbol{k}_{t1} \mathrm{sig}^{\alpha_c}(\boldsymbol{q}_{ti}) - \boldsymbol{k}_{t2} \mathrm{sig}^{\beta_e}(\boldsymbol{q}_{ti}) - \sum_{j=0}^{N} a_{ij} \dot{\psi}_i \boldsymbol{S} \begin{bmatrix} u_i \\ v_i \end{bmatrix} - \begin{bmatrix} 0 \\ \sum\limits_{j=0}^{N} a_{ij} v_i + \delta_0 \dot{\hat{\beta}}_i \end{bmatrix} + \\ & (\dot{\psi}_i \boldsymbol{S} + \boldsymbol{I}) \sum_{j=1}^{N} a_{ij} \boldsymbol{R}_i^{\mathrm{T}} \boldsymbol{R}_j \begin{bmatrix} u_j \\ v_j \end{bmatrix} + a_{i0} \boldsymbol{R}_i^{i} \dot{\boldsymbol{p}}_i + k_{vi} \Big(\sum_{j=0}^{N} a_{ij} \dot{\tilde{\boldsymbol{v}}}_i - \sum_{j=1}^{N} a_{ij} \boldsymbol{R}_i^{\mathrm{T}} \boldsymbol{R}_j \dot{\tilde{\boldsymbol{v}}}_j + a_{i0} \boldsymbol{R}_i^{\mathrm{T}} \ddot{\tilde{\boldsymbol{p}}}_i \Big)] \end{aligned} \tag{19}$$

where $0 < k_{vi} < 1$.

Remark 2: Based on the principle of PID controller, Eq. (19) can be regarded as a P, I, D type controller. The sideslip angle estimation can be regarded as the integral term, meanwhile the acceleration signals of $\dot{\boldsymbol{v}}_i$, $\dot{\boldsymbol{v}}_j$ and $\ddot{\boldsymbol{p}}_t$ in Eq. (19) can be regarded as differential terms. Filtering the acceleration signal also draws on

incomplete differential control technology, which can theoretically prove the rationality of the proposed method for smoothing the kinematic control output.

Remark 3: In order to further smooth the chattering signal brought by the acceleration signal to the kinematic control law, k_{vi} is set to reduce the chattering amplitude of the desired signal without sacrificing the convergence speed. It can also be regarded as a weight parameter to adjust the proportion of $\boldsymbol{e}_{pi}$ and $\boldsymbol{e}_{vi}$ in the system.

3.2 Fixed-time sliding mode controller

The following kinetic errors are defined:

$$\begin{cases} u_{ei} = u_{di} - u_i \\ r_{ei} = r_{di} - r_i \end{cases} \tag{20}$$

where u_{ei} is the surge velocity tracking error, u_{ei} is the yaw velocity tracking error.

Substituting Eq. (3) into the time derivative of Eq. (20) leads to:

$$\begin{cases} \dot{u}_{ei} = -\dfrac{\tau_{wui}}{m_{11,i}} - \dfrac{m_{22,i}}{m_{11,i}} v_i r_i + \dfrac{d_{11,i}}{m_{11,i}} u_i - \dfrac{d_{wui}}{m_{11,i}} + \dot{u}_{di} \\ \dot{r}_{ei} = -\dfrac{\tau_{wri}}{m_{33,i}} - \dfrac{m_{11,i} - m_{22,i}}{m_{33,i}} u_i v_i + \dfrac{d_{33,i}}{m_{33,i}} r_i - \dfrac{d_{wri}}{m_{33,i}} + \dot{r}_{di} \end{cases} \tag{21}$$

The CONN[23] is added to estimate the time-varying disturbance :

$$\boldsymbol{d}_{ti} = [\hat{d}_{wui}, \hat{d}_{wri}]^{\mathrm{T}} = \boldsymbol{W}_i^{\mathrm{T}} \boldsymbol{P}_{ij}(\boldsymbol{\xi}_i) + \boldsymbol{\varepsilon}_{wi} \qquad (j = 1, 2, ..., m_n) \tag{22}$$

$$\boldsymbol{P}_{ij}(\boldsymbol{\xi}_i) = \begin{cases} 1 & (j = 1) \\ \boldsymbol{g}(\boldsymbol{\xi}_i) & (j = 2) \\ 2\boldsymbol{g}(\boldsymbol{\xi}_i)\boldsymbol{P}_{i(j-1)}(\boldsymbol{\xi}_i) - \boldsymbol{P}_{i(j-2)}(\boldsymbol{\xi}_i) & (j = 3, ..., m_n) \end{cases} \tag{23}$$

where $\boldsymbol{W}_i = \begin{bmatrix} \boldsymbol{W}_{ui} & \boldsymbol{W}_{ri} \end{bmatrix}^{\mathrm{T}}$ denotes the weight vector, $\boldsymbol{P}_{ij}(\boldsymbol{\xi}_i)$ satisfies $\left\| \boldsymbol{P}_{ij}(\boldsymbol{\xi}_i) \right\| \leqslant \varsigma_{pi}$ with $\varsigma_{pi} > 0$, $\boldsymbol{\varepsilon}_{wi}$ is the approximation error, $\boldsymbol{\xi}_i = [u_{ei}, r_{ei}]^{\mathrm{T}}, \tilde{u}_i = u_{di} - u_i$, $\tilde{r}_i = r_{di} - r_i$, m_n is the number of nodes in the hidden layer of CONN, and $\boldsymbol{g}(\boldsymbol{\xi}_i) = 1/[1 + \exp(-\sum \boldsymbol{\xi}_i)]$.

The weight update law is given as follows:

$$\begin{cases} \hat{\boldsymbol{\tau}}_{ti}(k) = \hat{\boldsymbol{W}}_i^{\mathrm{T}} \boldsymbol{P}_{ij}(\boldsymbol{\xi}_i) \\ \dot{\hat{\boldsymbol{W}}}_i = \boldsymbol{\gamma}_i \boldsymbol{P}_{ij}(\boldsymbol{\xi}_i) \boldsymbol{\xi}_i - k_w \hat{\boldsymbol{W}}_i \end{cases} \tag{24}$$

where $\hat{\boldsymbol{W}}_i$ is the estimation value of weight vector, $\boldsymbol{\gamma}_i \in \Re^{m_n \times 1}$ is a positive parameter matrix, and k_w is a positive parameter.

Assumption 3: The weight vector $\boldsymbol{W}_i$ satisfies $\|\boldsymbol{W}_i\| \leqslant \overline{W}_i$, where $\overline{W}_i > 0$.

Substituting Eq. (24) into Eq. (21), it follows that:

$$\begin{cases} \dot{u}_{ei} = -\dfrac{\tau_{wui}}{m_{11,i}} + \hat{\Delta}_{ui} \\ \dot{r}_{ei} = -\dfrac{\tau_{wri}}{m_{33,i}} + \hat{\Delta}_{ri} \end{cases} \tag{25}$$

where $\hat{\Delta}_{ui} = -\dfrac{m_{22,i}}{m_{11,i}} v_i r_i + \dfrac{d_{11,i}}{m_{11,i}} u_i - \dfrac{\hat{\boldsymbol{W}}_{ui} \boldsymbol{P}_{ij}(\boldsymbol{\xi}_i)}{m_{11,i}} + \dot{u}_{di}$, $\hat{\Delta}_{ri} = -\dfrac{m_{11,i} - m_{22,i}}{m_{33,i}} u_i v_i + \dfrac{d_{33,i}}{m_{33,i}} r_i - \dfrac{\hat{\boldsymbol{W}}_{ri} \boldsymbol{P}_{ij}(\boldsymbol{\xi}_i)}{m_{33,i}} + \dot{r}_{di}$.

The fixed-time sliding surface is given as

$$\begin{cases} \dot{s}_{ui} = -k_{u1} \mathrm{sig}^{\alpha_u}(u_e) - k_{u2} \mathrm{sig}^{\beta_u}(u_e) \\ \dot{s}_{ri} = -k_{r1} \mathrm{sig}^{\alpha_r}(r_e) - k_{r2} \mathrm{sig}^{\beta_r}(r_e) \end{cases} \tag{26}$$

where k_{u1}, k_{u2}, k_{r1}, k_{r2} are positive gains, $0 < \alpha_u, \alpha_r < 1, \beta_u > 1, \beta_r > 1$.

Substituting Eq. (25) into Eq. (26), the fixed-time SMC is given as

$$\begin{cases} \tau_{ui} = m_{11,i}(k_{u1} \mathrm{sig}^{\alpha_u}(u_e) + k_{u2} \mathrm{sig}^{\beta_u}(u_e) + \hat{\Delta}_{ui}) \\ \tau_{ri} = m_{33,i}(k_{r1} \mathrm{sig}^{\alpha_r}(r_e) + k_{r2} \mathrm{sig}^{\beta_r}(r_e) + \hat{\Delta}_{ri}) \end{cases} \tag{27}$$

4 Stability analysis

The kinetic error subsystem is given as follows:

$$\begin{cases} \dot{s}_{ui} = -k_{u1}\mathrm{sig}^{\alpha_u}(u_{ei}) - k_{u2}\mathrm{sig}^{\beta_u}(u_{ei}) \\ \dot{s}_{ri} = -k_{r1}\mathrm{sig}^{\alpha_r}(r_{ei}) - k_{r2}\mathrm{sig}^{\beta_r}(r_{ei}) \\ \dot{\tilde{\boldsymbol{W}}}_i = -k_w\tilde{\boldsymbol{W}}_i \end{cases} \tag{28}$$

Theorem 1: If Assumption 3 holds, the tracking errors of $\tilde{u}_{ei}$, $\tilde{r}_{ei}$ and $\tilde{\boldsymbol{W}}_i$ in Eq. (28) will converge in a fixed time by choosing $k_{u1}, k_{u2}, k_{r1}, k_{r2}, k_w$ appropriately.

Proof: A Lyapunov function is given as follows:

$$\boldsymbol{V}_{t_1} = \frac{1}{2}u_{ei}^2 + \frac{1}{2}r_{ei}^2 + \gamma_i^{-1}k_w\tilde{\boldsymbol{W}}_i^{\mathrm{T}}\tilde{\boldsymbol{W}}_i \tag{29}$$

The differentiation of Eq. (29) is as follows:

$$\begin{aligned} \dot{\boldsymbol{V}}_{t_1} &= u_{ei}(-k_{u1}\mathrm{sig}^{\alpha_u}(u_e) - k_{u2}\mathrm{sig}^{\beta_u}(u_e)) + r_{ei}(-k_{r1}\mathrm{sig}^{\alpha_r}(r_e) - k_{r2}\mathrm{sig}^{\beta_r}(r_e)) + \gamma_i^{-1}k_w\tilde{\boldsymbol{W}}_i^{\mathrm{T}}\dot{\tilde{\boldsymbol{W}}}_i \\ &\leqslant -k_{u1}\|u_{ei}\|^{\alpha_u+1} - k_{u2}\|u_{ei}\|^{\beta_u+1} - k_{r1}\|r_{ei}\|^{\alpha_r+1} - k_{r2}\|r_{ei}\|^{\beta_r+1} - k_w\gamma_i^{-1}\tilde{\boldsymbol{W}}_i^2 + \gamma_i^{-1}k_w\tilde{\boldsymbol{W}}_i^{\mathrm{T}}\dot{\tilde{\boldsymbol{W}}}_i \\ &= -k_{u1}\|u_{ei}\|^{\alpha_u+1} + k_{r1}\|r_{ei}\|^{\alpha_r+1} + \frac{1}{2}k_w\gamma_i^{-1}\left\|\tilde{\boldsymbol{W}}_i\right\|^{\alpha_w+1} - k_{u2}\|u_{ei}\|^{\beta_u+1} + k_{r2}\|r_{ei}\|^{\beta_r+1} + \\ &\frac{1}{2}k_w\gamma_i^{-1}\left\|\tilde{\boldsymbol{W}}_i\right\|^{\beta_w+1} + 2\lambda_{\min}(\boldsymbol{P}_{ij})\bar{\boldsymbol{\varepsilon}}_{wi} + k_w\gamma_i^{-1}\bar{\boldsymbol{W}}_i^2 \leqslant -\boldsymbol{A}_{t_1}\boldsymbol{E}_{t_1}^{\frac{\alpha_{t_1}+1}{2}} - \boldsymbol{B}_{t_1}\boldsymbol{E}_{t_1}^{\frac{\beta_{t_1}+1}{2}} + \|\boldsymbol{H}_1\| \end{aligned} \tag{30}$$

where $\boldsymbol{A}_{t_1} = \mathrm{diag}[k_{u1}, k_{r1}, \frac{1}{2}k_w\gamma_i^{\frac{\alpha_w-1}{2}}\left\|\tilde{\boldsymbol{W}}_i\right\|^{1-\alpha_w}]$, $\boldsymbol{B}_{t_1} = \mathrm{diag}[k_{u2}, k_{r2}, \frac{1}{2}k_w\gamma_i^{\frac{\beta_w-1}{2}}\left\|\tilde{\boldsymbol{W}}_i\right\|^{1-\beta_w}]$, $\boldsymbol{E}_{t_1} = [\|u_{ei}\|^2, \|u_{ri}\|^2, \gamma_i^{-1}\left\|\tilde{\boldsymbol{W}}_i\right\|^2]^{\mathrm{T}}$, $\boldsymbol{H}_1 = 2\lambda_{\min}(\boldsymbol{P}_{ij})\bar{\boldsymbol{\varepsilon}}_{wi} + k_w\gamma_i^{-1}\bar{\boldsymbol{W}}_i^2$, $\alpha_{t_1} = \min\{\alpha_u, \alpha_r, \alpha_w\}$, and $\beta_{t_1} = \min\{\beta_u, \beta_r, \beta_w\}$.

Eq. (30) can be rewritten as follows:

$$\dot{\boldsymbol{V}}_{t_1} \leqslant -\boldsymbol{A}_{t_1}\boldsymbol{V}_{t_1}^{\frac{\alpha_{t_1}+1}{2}} - \boldsymbol{B}_{t_1}\boldsymbol{V}_{t_1}^{\frac{\beta_{t_1}+1}{2}} + \|\boldsymbol{H}_1\| \tag{31}$$

Applying Lemma 1, the error $\boldsymbol{E}_{t_1}$ will converge in a fixed-time T_1 satisfying

$$T_1 \leqslant \frac{2}{\boldsymbol{A}_{t_1}\varepsilon_3(1-a_{t_1})} + \frac{2}{\boldsymbol{B}_{t_1}\varepsilon_3(\beta_{t_1}-1)} \tag{32}$$

$\boldsymbol{e}_z = \boldsymbol{v}_z - \tilde{\boldsymbol{v}}_z$ is defined as the filter error, its derivative is taken and substituted into Eq. (21), it follows that:

$$\dot{\boldsymbol{e}}_z = \dot{\boldsymbol{v}}_z - T_d^{-1}\boldsymbol{e}_z \tag{33}$$

$\boldsymbol{B}_{2i} = \sum_{j=0}^{N} a_{ij}\dot{\psi}_i\boldsymbol{S}$ is defined, substituting Eq. (19) into Eq. (14) and combining Eq. (16), the kinematic error subsystem can be given as follows:

$$\begin{cases} \dot{\bar{\boldsymbol{e}}}_{ti} = -\dot{\psi}_i\boldsymbol{S}\bar{\boldsymbol{e}}_{ti} - \boldsymbol{k}_{t1}\mathrm{sig}^{\alpha_t}(\boldsymbol{q}_{ti}) - \boldsymbol{k}_{t2}\mathrm{sig}^{\beta_t}(\boldsymbol{q}_{ti}) + \boldsymbol{B}_{2i}\tilde{\boldsymbol{v}}_i \\ \dot{\boldsymbol{e}}_z = \dot{\boldsymbol{v}}_z - T_d^{-1}\boldsymbol{e}_z \\ \dot{\tilde{\boldsymbol{Z}}}_i = \boldsymbol{A}_{\psi i}[\mathrm{sig}^{\alpha_\psi}(z_{1i}) + \mathrm{sig}^{\beta_\psi}(z_{1i}), z_{2i}]^{\mathrm{T}} \\ \boldsymbol{A}_{\psi i} = \begin{bmatrix} -k_{1i} & 1 \\ -k_{2i} & 0 \end{bmatrix} \end{cases} \tag{34}$$

where $\tilde{\boldsymbol{Z}}_i = [z_{1i}, z_{2i}]^{\mathrm{T}}$, $\boldsymbol{k}_e = \boldsymbol{k}_{e1} + \boldsymbol{k}_{e2}$, $\boldsymbol{A}_{\psi i}$ is a Hurwitz matrix such that $\boldsymbol{A}_{\psi i}^{\mathrm{T}}\boldsymbol{P}_{\psi i} + \boldsymbol{P}_{\psi i}\boldsymbol{A}_{\psi i} = -\boldsymbol{I}$, $\boldsymbol{P}_{\psi i}$ is a positive matrix.

Theorem 2: If Assumptions 1–2 and Theorem 1 hold, the tracking errors of $\bar{\boldsymbol{e}}_{ti}$, $\boldsymbol{e}_z$ and $\tilde{\boldsymbol{Z}}_i$ in Eq. (34) will converge in a fixed time, where $\boldsymbol{k}_{t1}$ and T_d need to satisfy $\boldsymbol{k}_{t1} > \max\{\|\boldsymbol{H}_1\|\|\bar{\boldsymbol{e}}_{ti}\|^{1-\alpha_{t1}}, 0\}$ and $0 < T_d < 2$, which are later defined in Eq. (36).

Proof: A Lyapunov function is given as follows:

$$\boldsymbol{V}_{t_2} = \bar{\boldsymbol{e}}_{ti}^{\mathrm{T}}\bar{\boldsymbol{e}}_{ti} + \boldsymbol{e}_z^{\mathrm{T}}\boldsymbol{e}_z + \tilde{\boldsymbol{Z}}_i^{\mathrm{T}}\boldsymbol{P}_{\psi i}\tilde{\boldsymbol{Z}}_i \tag{35}$$

The substitution of Eq. (34) into the differentiation of Eq. (35) is as follows:

$$\begin{aligned}\dot{\boldsymbol{V}}_{t_2}=&-\dot{\psi}_i\boldsymbol{S}\|\bar{\boldsymbol{e}}_{ti}\|^2-\boldsymbol{k}_{t1}\|\bar{\boldsymbol{e}}_{ti}\|^{\alpha_t+1}-\boldsymbol{k}_{t2}\|\bar{\boldsymbol{e}}_{ti}\|^{\beta_t+1}+\boldsymbol{k}_{t2}\mathrm{sig}^{\beta_t}(\bar{\boldsymbol{e}}_{fi})\bar{\boldsymbol{e}}_{ti}+\boldsymbol{B}_{2i}\tilde{\boldsymbol{v}}_i\bar{\boldsymbol{e}}_{ti}-T_d^{-1}\|\boldsymbol{e}_z\|^2+\boldsymbol{e}_z\dot{\boldsymbol{v}}_z+\\&\boldsymbol{k}_{t1}\mathrm{sig}^{\alpha_t}(\bar{\boldsymbol{e}}_{fi})\bar{\boldsymbol{e}}_{ti}+\tilde{\boldsymbol{Z}}_i^{\mathrm{T}}(\boldsymbol{P}_{\psi i}\boldsymbol{A}_{\psi i}+\boldsymbol{A}_{\psi i}^{\mathrm{T}}\boldsymbol{P}_{\psi i})\tilde{\boldsymbol{Z}}_i\leqslant(\boldsymbol{B}_{2i}-\dot{\psi}_i\boldsymbol{S}+\frac{1}{2}\boldsymbol{k}_{t1}+\frac{1}{2}\boldsymbol{k}_{t2})\|\bar{\boldsymbol{e}}_{ti}\|^2+\frac{1}{2}\boldsymbol{k}_{t1}\left\|\bar{\boldsymbol{e}}_{fi}\right\|^{2\alpha_t+2}+\\&\frac{1}{2}\boldsymbol{k}_{t2}\left\|\bar{\boldsymbol{e}}_{fi}\right\|^{2\beta_t+2}-\boldsymbol{k}_{t1}\|\bar{\boldsymbol{e}}_{ti}\|^{\alpha_t+1}-\boldsymbol{k}_{t2}\|\bar{\boldsymbol{e}}_{ti}\|^{\beta_t+1}-(T_d^{-1}-\frac{1}{2})\|\boldsymbol{e}_z\|^2+\frac{1}{2}\|\dot{\boldsymbol{v}}_z\|^2-\left\|\tilde{\boldsymbol{Z}}_i\right\|^2+\boldsymbol{B}_{2i}\|\tilde{\boldsymbol{v}}_i\|^2\end{aligned}\tag{36}$$

Considering that $\dot{\boldsymbol{v}}_z$ is a continuous vector, it satisfies $\dot{\boldsymbol{v}}_z\leqslant\boldsymbol{v}_z^*$, where $\boldsymbol{v}_z^*=[v_u^*,v_r^*]^{\mathrm{T}}$, v_u^* and v_r^* are positive constants.

Defining $\boldsymbol{H}_1=\boldsymbol{B}_{2i}-\dot{\psi}_i\boldsymbol{S}+\frac{1}{2}\boldsymbol{k}_{t1}+\frac{1}{2}\boldsymbol{k}_{t2}$, $H_2=T_d^{-1}-\frac{1}{2}$, $\boldsymbol{H}_3=\frac{1}{2}\boldsymbol{k}_{t1}\left\|\bar{\boldsymbol{e}}_{fi}\right\|^{2\alpha_t+2}+\frac{1}{2}\boldsymbol{k}_{t2}\left\|\bar{\boldsymbol{e}}_{fi}\right\|^{2\beta_t+2}$, Eq. (36) can be given as follows:

$$\begin{aligned}\dot{\boldsymbol{V}}_{t_2}=&-\boldsymbol{k}_{t1}\|\bar{\boldsymbol{e}}_{ti}\|^{\alpha_t+1}-\boldsymbol{k}_{t2}\|\bar{\boldsymbol{e}}_{ti}\|^{\beta_t+1}+\boldsymbol{H}_1\|\bar{\boldsymbol{e}}_{ti}\|^2+\boldsymbol{B}_{2i}\|\tilde{\boldsymbol{v}}_i\|^2-H_2\|\boldsymbol{e}_z\|^2+\frac{1}{2}\left\|\boldsymbol{v}_z^*\right\|^2-\left\|\tilde{\boldsymbol{Z}}_i\right\|^2+\boldsymbol{H}_3\leqslant\\&-\boldsymbol{k}_{t1}\|\bar{\boldsymbol{e}}_{ti}\|^{\alpha_t+1}-\boldsymbol{k}_{t2}\|\bar{\boldsymbol{e}}_{ti}\|^{\beta_t+1}-H_2\|\boldsymbol{e}_z\|^2+\boldsymbol{B}_{2i}\|\tilde{\boldsymbol{v}}_i\|^2+\|\boldsymbol{H}_1\|\,\|\bar{\boldsymbol{e}}_{ti}\|^{1-\alpha_t}\|\bar{\boldsymbol{e}}_{ti}\|^{\alpha_t+1}+\frac{1}{2}\left\|\boldsymbol{v}_z^*\right\|^2-\left\|\tilde{\boldsymbol{Z}}_i\right\|^2+\|\boldsymbol{H}_3\|=\\&-(\boldsymbol{k}_{t1}-\|\boldsymbol{H}_1\|\,\|\bar{\boldsymbol{e}}_{ti}\|^{1-\alpha_t})\|\bar{\boldsymbol{e}}_{ti}\|^{\alpha_t+1}-\boldsymbol{k}_{t2}\|\bar{\boldsymbol{e}}_{ti}\|^{\beta_t+1}-\frac{H_2\|\boldsymbol{e}_z\|^{1-\alpha_z}}{2}\|\boldsymbol{e}_z\|^{\alpha_z+1}-\frac{H_2\|\boldsymbol{e}_z\|^{1-\beta_z}}{2}\|\boldsymbol{e}_z\|^{\beta_z+1}-\\&\frac{\left\|\tilde{\boldsymbol{Z}}_i\right\|^{1-\alpha_\psi}}{2}\left\|\tilde{\boldsymbol{Z}}_i\right\|^{\alpha_\psi+1}-\frac{\left\|\tilde{\boldsymbol{Z}}_i\right\|^{1-\beta_\psi}}{2}\left\|\tilde{\boldsymbol{Z}}_i\right\|^{\beta_\psi+1}+\frac{1}{2}\left\|\boldsymbol{v}_z^*\right\|^2+\boldsymbol{B}_{2i}\|\tilde{\boldsymbol{v}}_i\|^2+\|\boldsymbol{H}_3\|\\=&-\boldsymbol{A}_{t_2}\boldsymbol{E}_{t_2}^{\frac{\alpha_{t_2}+1}{2}}-\boldsymbol{B}_{t_2}\boldsymbol{E}_{t_2}^{\frac{\beta_{t_2}+1}{2}}+\boldsymbol{H}_4\end{aligned}\tag{37}$$

where $\boldsymbol{A}_{t_2}=\mathrm{diag}[\boldsymbol{k}_{t1}-\|\boldsymbol{H}_1\|\,\|\bar{\boldsymbol{e}}_{ti}\|^{1-\alpha_t};-\frac{1}{2}H_2\|\boldsymbol{e}_z\|^{1-\alpha_z};\frac{1}{2}\boldsymbol{p}_{\psi i}^{\frac{-\alpha_\psi-1}{2}}\left\|\tilde{\boldsymbol{Z}}_i\right\|^{1-\alpha_\psi}]$, $\boldsymbol{E}_{t_2}=[\left\|\bar{\boldsymbol{e}}_{pi}\right\|^2,\boldsymbol{p}_{\psi i}\left\|\tilde{\boldsymbol{Z}}_i\right\|^2]^{\mathrm{T}}$. $\boldsymbol{B}_{t_2}=\mathrm{diag}[\boldsymbol{k}_{t2};-\frac{1}{2}H_2\|\boldsymbol{e}_z\|^{1-\beta_z};\frac{1}{2}\boldsymbol{p}_{\psi i}^{\frac{-\beta_\psi-1}{2}}\left\|\tilde{\boldsymbol{Z}}_i\right\|^{1-\beta_\psi}]$, $\alpha_{t_2}=\min\{\alpha_t,\alpha_z,\alpha_\psi\}$, $\beta_{t_2}=\min\{\beta_t,\beta_z,\beta_\psi\}$, $\boldsymbol{H}_4=\boldsymbol{B}_{2i}\|\tilde{\boldsymbol{v}}_i\|^2+\frac{1}{2}\left\|\boldsymbol{v}_z^*\right\|^2+\|\boldsymbol{H}_3\|$.

According to Theorem 1, $\tilde{\boldsymbol{v}}_i$ can eventually converge to 0. From Eq. (37), when $\boldsymbol{k}_{t1}>\max\{\|\boldsymbol{H}_1\|\,\|\bar{\boldsymbol{e}}_{ti}\|^{1-\alpha_t},0\}$, $0<T_d<2$, it follows that:

$$\dot{\boldsymbol{V}}_{t_2}\leqslant-\boldsymbol{A}_{t_2}\boldsymbol{V}_{t_2}^{\frac{\alpha_{t2}+1}{2}}-\boldsymbol{B}_{t_2}\boldsymbol{V}_{t_2}^{\frac{\beta_{t2}+1}{2}}+\|\boldsymbol{H}_4\|\tag{38}$$

Applying Lemma 1, the error $\boldsymbol{E}_{t_2}$ will converge in a fixed-time T_2 satisfying

$$T_2\leqslant\frac{2}{\boldsymbol{A}_{t_2}\varepsilon_3(1-a_{t_2})}+\frac{2}{\boldsymbol{B}_{t_2}\varepsilon_3(\beta_{t_2}-1)}\tag{39}$$

To sum up, the tracking errors of the whole TACC control system converge in a fixed-time T_3 satisfying

$$T_3\leqslant\max\{\frac{2}{\boldsymbol{A}_{t_2}\varepsilon_3(1-a_{t_2})}+\frac{2}{\boldsymbol{B}_{t_2}\varepsilon_3(\beta_{t_2}-1)},\frac{2}{\boldsymbol{A}_{t_1}\varepsilon_3(1-a_{t_1})}+\frac{2}{\boldsymbol{B}_{t_1}\varepsilon_3(\beta_{t_1}-1)}\}\tag{40}$$

5 Simulation results

In this chapter, four USVs and one moving target are considered, where status information of the non-cooperative target can be directly obtained by a USV shown in Fig. 3. The effects of the two cooperative kinematics control laws of Eqs. (17) and (19) on the proposed TACC control system are compared, respectively. The initial position of the target is set as $\boldsymbol{p}_t=[10\text{ m},10\text{ m},0^\circ]^{\mathrm{T}}$. The velocity of the target is set as $\boldsymbol{v}_t=[1\text{ m/s},0\text{ m/s},0.0045\times\sin(0.001\times T)\text{ rad/s}]^{\mathrm{T}}$, where T is the number of control cycles. The initial position of USVs are given as $\boldsymbol{p}_1=[-10\text{ m},-20\text{ m},0^\circ]^{\mathrm{T}}$, $\boldsymbol{p}_2=[-10\text{ m},0\text{ m},0^\circ]^{\mathrm{T}}$, $\boldsymbol{p}_3=[-10\text{ m},20\text{ m},0^\circ]^{\mathrm{T}}$, and $\boldsymbol{p}_4=[-20\text{ m},0\text{ m},0^\circ]^{\mathrm{T}}$. The initial velocity of USVs are all set as $\boldsymbol{v}_i=[0.2\text{ m/s},0\text{ m/s},0\text{ rad/s}]^{\mathrm{T}}$. The mathematical model of USVs are the same as in Ref. [24]. The main simulation parameters are shown in Tab. 1.

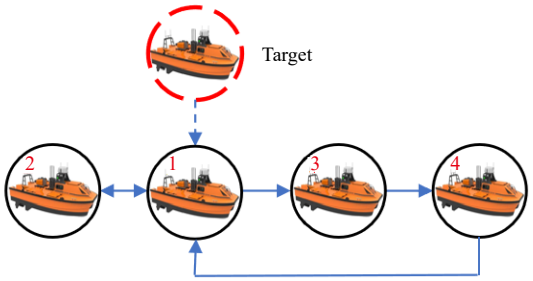

Fig.3 Communication topology of the networked system

Tab.1 Main simulation parameters

Kinematic control parameters				SigAPF parameters				Kinetic control parameters			
Symbol	Value	Symbol	Value	Symbol	Value	Symbol	Value	Symbol	Value	Symbol	Value
N	4	δ_0	0.15	R_{a1}/m	9	R_{a2}/m	5	k_{u1}	1.2	k_{u2}	1.2
$\boldsymbol{k}_{t1}$	diag[0.4;0.15]	$\boldsymbol{k}_{t2}$	diag[0.4;0.15]	R_{c1}/m	100	R_{c2}/m	70	k_{r1}	0.3	k_{r2}	0.3
α_t	0.8	β_t	1.2	ε_{ia}	0.005	c_{ia}	0.1	α_u	0.7	α_r	0.7
k_{i1}	10	k_{i2}	20	ε_{ic}	0.001	c_{ic}	0.5	β_u	1.5	β_r	1.5
α_ψ	0.8	β_ψ	1.2					γ_i	$0.1\times\text{diag}[1;1;1;1;1]$	k_w	10^{-4}
T_d	0.5	k_{vi}	0.1					$\boldsymbol{W}_i$	$0\times\Re^{3\times5}$		

Fig. 4 shows the trajectories of the target and 4 USVs. The four USVs are conducting coordinated patrol missions in a certain formation and initial velocity at the initial moment, and immediately carry out target tracking missions after discovering the target, and each USV is allocated to its own tracking point. After a period of time, USVs quickly change from a triangle formation to a semi-enclosed formation, and the tracking formation is always maintained during subsequent movements. Fig. 5 presents the position tracking errors between USVs and tracking points. After 50 s, the USVs position tracking errors achieve convergence. And the post-convergence mean square errors (MSE) are 0.94 m, 0.83 m, 1.03 m and 1.09 m respectively. The velocity tracking errors between USVs and the target is shown in Fig. 6. The USVs

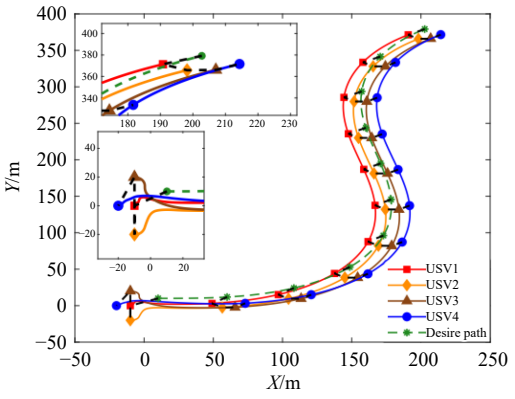

Fig.4 Trajectories of the target and 4 USVs, and their snapshots

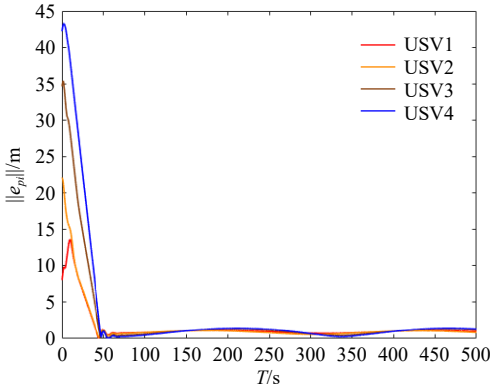

Fig.5 Position tracking errors between USVs and tracking points

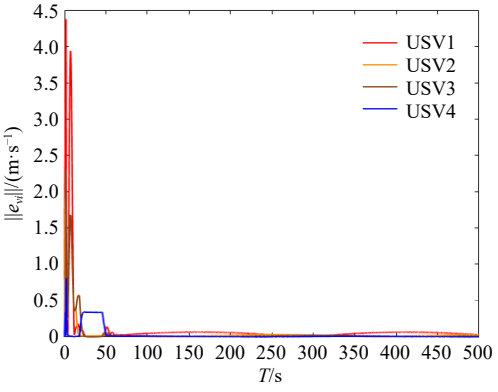

Fig.6 Velocity tracking errors between USVs and the target

velocity tracking errors achieve convergence like the position tracking errors, and the MSE are 0.14 m/s, 0.0325 m/s, 0.0329 m/s and 0.0077 m/s respectively. The result in Fig. 6 further proves the rationality of Remarks 3–4.

Fig. 7 and Fig. 8 show the compared results of the control method with and without DSC in desired velocity tracking and kinetic control output respectively. In Fig. 7, the control method with DSC and the control method without DSC can both converge the actual velocity to the desired kinematic control output. However, the control method with DSC smoothes the chattering of the desired velocity signal, so that the actual velocity signal is also optimized. The result in Fig. 7 is further reflected in Fig. 8. The control method without DSC has a maximum amplitude of 20 N on the surge control output and a trend of gradually increasing and diverging, and a maximum amplitude of 0.6 N·m on the yaw control output. In comparison, the output of the control method with DSC is greatly optimized, which is more conducive to practical engineering applications.

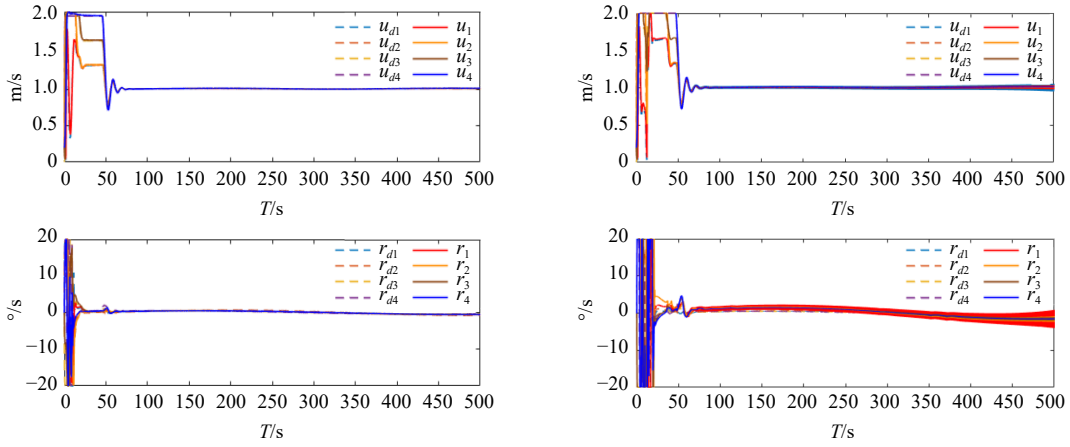

（a）With DSC　　（b）Without DSC

Fig.7 Velocity tracking performance with and without DSC

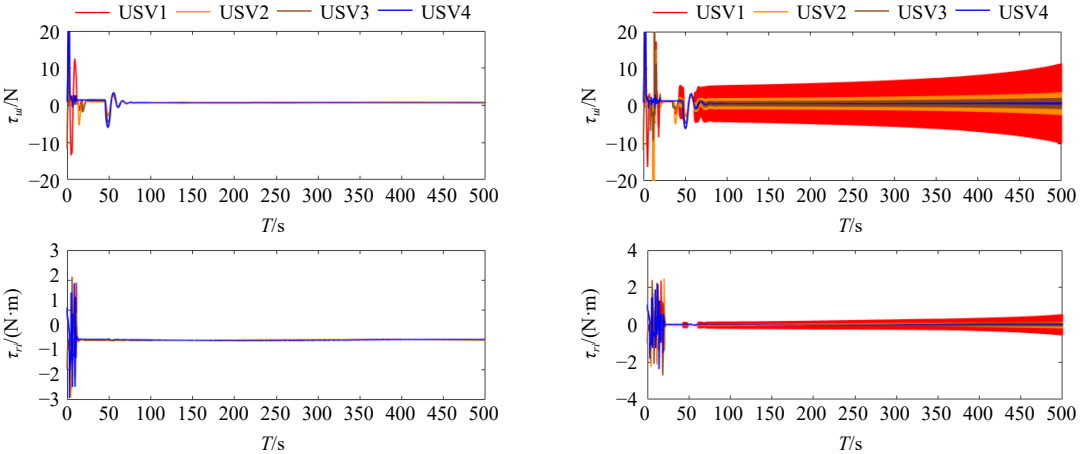

（a）With DSC　　（a）Without DSC

Fig.8 Control outputs with and without DSC

Fig. 9 shows the results of APFs. In the first 50 s, there is a risk of collision when the USVs move towards their respective tracking points. Under the inter-USVs collision avoidance APF, the navigation safety of the USVs is guaranteed. Fig. 10 and Fig. 11 show the verification of the effectiveness of the fixed-time

ESO and CONN estimator in estimating time-varying sideslip angle and external environmental disturbance respectively.

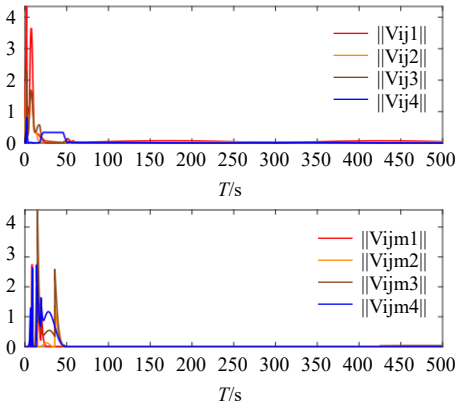

Fig.9 APF values of inter-USVs collision avoidance and connectivity constraint

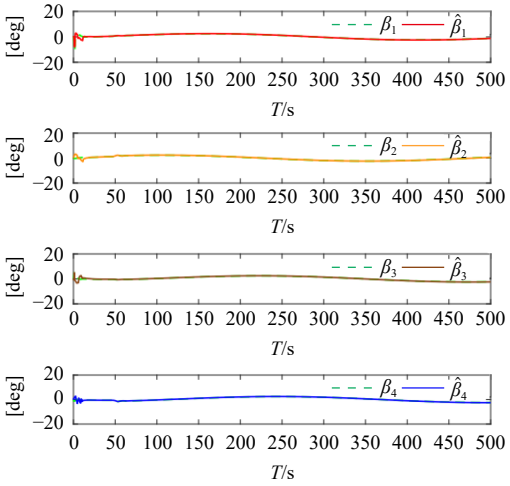

Fig.10 Sideslip angle estimation results

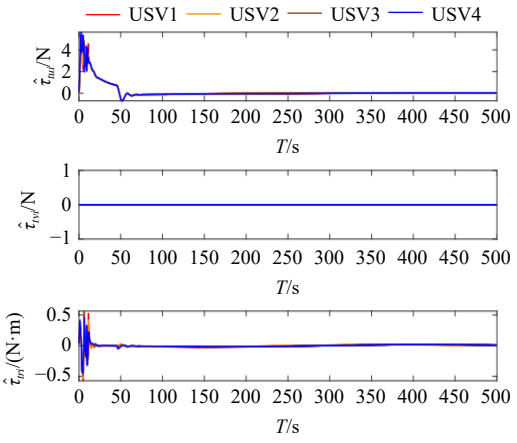

Fig.11 Time-varying disturbance estimation results

6 Concluding remarks

In this paper, semi-encirclement TACC of USVs under maritime security conditions is studied, and a novel fixed-time TACC approach is proposed. Firstly, A decoupled TACC control structure is designed, and the independent debugging of kinematic control law and kinetic control law is more suitable for practical engineering applications and reduces the complexity of system design. Secondly, a DSC-based target-guided kinematic control law including tracking points pre-allocation strategy and sigmoid-APFs is proposed, where collision avoidance during target tracking is effectively achieved by using sigmoid-APFs. Simultaneously, dynamic surface control technology greatly optimizes the subsequent control output. Finally, a fixed-time TACC system is proposed for the first time. In the kinetic layer, the designed fixed-time sliding mode controller combined with CONN can achieve fast convergence of control errors and achieve accurate compensation of time-varying sideslip angle and external environmental disturbance simultaneously. The effectiveness of the proposed TACC approach in improving target tracking safety and reducing control output chattering is verified by the simulation comparison results.

Currently, the situation where tracking points are dynamically allocated due to non-cooperative target movement or changes in the navigation environment is not considered in this paper. In addition, it is ideal to assume that the target state can be obtained by some USVs. Combined with the real detection range of the sensors mounted on USVs, state estimation of the target under switching topology is another research content in the future.

References

[1] Gu N, Wang D, Peng Z, et al. Advances in line-of-sight guidance for path following of autonomous marine vehicles: An overview[J]. IEEE Transactions on Systems, Man, and Cybernetics: Systems, 2023, 53(1): 12–28.

[2] Er M, Ma C, Liu, T, et al. Intelligent motion control of unmanned surface vehicles: A critical review[J]. Ocean Engineering, 2023, 280(0): 114562.

[3] Liu L, Wang D, Peng Z. ESO-based line-of-sight guidance law for path following of underactuated marine surface vehicles with exact sideslip compensation[J]. IEEE Journal of Oceanic Engineering, 2017, 42(2): 477–487.

[4] Fu M, Yu L. Finite-time extended state observer-based distributed formation control for marine surface vehicles with input saturation and disturbances[J]. Ocean Engineering, 2018, 159(0): 219–227.

[5] Bong S, Sung J. An error transformation approach for connectivity-preserving and collision-avoiding formation tracking of networked uncertain underactuated surface vessels[J]. IEEE Transactions on Cybernetics, 2019, 49(8): 2955–2966.

[6] Peng Z, Wang J, Wang, D, et al. An overview of recent advances in coordinated control of multiple autonomous surface vehicles[J]. IEEE Transactions on Industrial Informatics, 2021, 17(2): 732–745.

[7] Hu B, Zhang H. Bearing-only motional target-surrounding control for multiple unmanned surface vessels[J]. IEEE Transactions on Industrial Electronics, 2022, 69(4): 3988–3997.

[8] Hu B, Zhang H, Liu B, et al. Distributed surrounding control of multiple unmanned surface vessels with varying interconnection topologies[J]. IEEE Transactions on Control Systems Technology, 2022, 30(1): 400–407.

[9] Fahimi F. Sliding-mode formation control for underactuated surface vessels[J]. IEEE Transactions on Robotics, 2007, 23(3): 617–622.

[10] Peng Z, Wang D, Chen Z, et al. Adaptive dynamic surface control for formations of autonomous surface vehicles with uncertain dynamics[J]. IEEE Transactions on Control Systems Technology, 2013, 21(2): 513–520.

[11] Khoshnam S. Leader-follower formation control of underactuated autonomous marine surface vehicles with limited torque[J]. Ocean Engineering, 2015, 105(0): 196–205.

[12] Xu J. Fault-tolerant finite-time leader-follower formation control for autonomous surface vessels with LOS range and angle constraints[J]. Automatica, 2016, 68(0): 228–236.

[13] Sun Z. Zhang G, Lu Y, et al. Leader-follower formation control of underactuated surface vehicles based on sliding mode control and parameter estimation[J]. ISA Transactions, 2018, 72(0): 15–24.

[14] Liu L, Wang D, Peng Z, et al. Bounded neural network control for target tracking of underactuated autonomous surface vehicles in the presence of uncertain target dynamics[J]. IEEE Transactions on Neural Networks and Learning Systems, 2019, 30(4): 1241–1249.

[15] Gao S, Peng Z, Liu L, et al. Coordinated target tracking by multiple unmanned surface vehicles with communication delays based on a distributed event-triggered extended state observer[J]. Ocean Engineering, 2021, 227(0): 108283.

[16] Gao S, Peng Z, Wang H, et al. Safety-critical model-free control for multi-target tracking of USVs with collision avoidance[J]. IEEE/CAA Journal of Automatica Sinica, 2022, 9(7): 1323–1326.

[17] Qian G, Zheng X, Wang J, et al. Equilateral triangular formation of unmanned surface vehicles for target tracking with event-triggered collision avoidance[J]. Ocean Engineering, 2023, 267(0): 113211.

[18] Ma L, Wang Y, Han Q. Cooperative target tracking of multiple autonomous surface vehicles under switching interaction topologies[J]. IEEE/CAA Journal of Automatica Sinica, 2023, 10(3): 673–684.

[19] Zhu Y, Bai J, Guo G. Cooperative target substitution tracking control of multiple unmanned surface vehicles with substitute

USVs[J]. Ocean Engineering, 2023, 273(0): 113903.
[20] Zhu Y, Bai J, Li S, et al. Selection strategies and finite-time target tracking of multiple unmanned surface vehicles with mode uncertainty and disturbances[J]. Ocean Engineering, 2023, 283(0): 115088.
[21] Michael B. Finite- and fixed-time convergent algorithms: Design and convergence time estimation[J]. Annual Reviews in Control, 2019, 48(0): 209–221.
[22] Li C, Xu H, Yu W, et al. Exponential smoothing-based fixed-time path-guided coordinated control of unmanned surface vehicles under communication interruption[J]. Ocean Engineering, 2024, 298(0): 117119.
[23] Yu W, Xu H, Han X, et al. Fault-tolerant control for dynamic positioning vessel with thruster faults based on the neural modified extended state observer[J]. IEEE Transactions on Systems, Man and Cybernetics: Systems, 2021, 51(9): 5905–5917.
[24] Liang X, Qu X, Wang N, et al. Swarm control with collision avoidance for multiple underactuated surface vehicles[J]. Ocean Engineering, 2019, 4(0): 106516.

基于动态面技术的固定时间多无人艇分布式目标跟踪控制

李超逸[2], 徐海祥[1,2,3], 余文曌[1,2,3], 杜　哲[1,2], 丁亚楠[2]
（1. 高性能船舶技术教育部重点实验室(武汉理工大学), 武汉 430062; 2. 武汉理工大学 船海与能源动力工程学院, 武汉 430062; 3. 武汉理工大学 三亚科教创新园, 海南 三亚 572024）

摘要: 本文针对多无人艇分布式目标跟踪控制问题进行研究。在跟踪非合作目标的场景下, 只有部分个体能够获取目标的状态信息。为了实现对非合作目标的快速安全跟踪, 本文提出一种基于动态面控制的固定时间跟踪控制方法。首先, 设计一种运动学和动力学解耦的分布式目标跟踪控制结构, 以降低控制系统设计的复杂度。其次, 提出一种基于动态面技术的运动学控制律, 其中包含跟踪点预分配策略和避碰势场函数, 可在跟踪过程中避免碰撞并优化运动学控制输出。最后, 提出一种固定时间分布式目标跟踪控制系统, 实现运动学和动力学误差的快速收敛。仿真对比结果验证了本文所提方法在提高目标跟踪安全性和减少控制输出抖振方面的有效性。

关键词: 多无人艇; 分布式控制; 目标跟踪控制; 固定时间收敛; 动态面控制
中图分类号: TP273　U664.82　　**文献标识码:** A
基金项目: 国家自然科学基金资助项目(52201373); 海南省科技计划三亚崖州湾科技城科技创新联合项目(2021CXLH0016)

作者简介: 李超逸(1996–), 男, 博士研究生;
徐海祥(1975–), 男, 博士, 武汉理工大学教授;
余文曌(1989–), 男, 博士, 武汉理工大学副研究员;
杜　哲(1993–), 男, 博士, 武汉理工大学讲师;
丁亚楠(1998–), 女, 硕士研究生。